HHS Public Access

Author manuscript

Oncogene. Author manuscript; available in PMC 2022 July 03.

Published in final edited form as:

Oncogene. 2022 February ; 41(6): 852–864. doi:10.1038/s41388-021-02135-3.

RB1 loss in castration-resistant prostate cancer confers vulnerability to LSD1 inhibition

Wanting Han[1,2,*], **Mingyu Liu**[1,2,*], **Dong Han**[1], **Muqing Li**[1,2], **Anthia A Toure**[1,2], **Zifeng Wang**[1,2], **Anna Besschetnova**[1,2], **Susan Patalano**[1,2], **Jill A. Macoska**[1,2], **Shuai Gao**[1,2], **Housheng Hansen He**[3,4], **Changmeng Cai**[1,2]

[1]Center for Personalized Cancer Therapy, University of Massachusetts Boston, Boston, Massachusetts 02125, USA

[2]Department of Biology, University of Massachusetts Boston, Boston, Massachusetts 02125, USA

[3]Department of Medical Biophysics, University of Toronto, Toronto, Canada

[4]Princess Margaret Cancer Center, University Health Network, Toronto, Ontario, M5G1L7, Canada

Abstract

Genomic loss of *RB1* is a common alteration in castration-resistant prostate cancer (CRPC) and is associated with poor patient outcomes. *RB1* loss is also a critical event that promotes the neuroendocrine transdifferentiation of prostate cancer (PCa) induced by the androgen receptor (AR) signaling inhibition (ARSi). The loss of Rb protein disrupts the Rb-E2F repressor complex and thus hyperactivates E2F transcription activators. While the impact of Rb inactivation on PCa progression and linage plasticity has been previously studied, there is a pressing need to fully understand underlying mechanisms and identify vulnerabilities that can be therapeutically targeted in Rb-deficient CRPC. Using an integrated cistromic and transcriptomic analysis, we have characterized Rb activities in multiple CRPC models by identifying Rb directly regulated genes and revealed that Rb has distinct binding sites and targets in CRPC with different genomic backgrounds. Significantly, we show that E2F1 chromatin binding and transcription activity in Rb-deficient CRPC are highly dependent on LSD1/KDM1A, and that Rb inactivation sensitizes CRPC tumor to the LSD1 inhibitor treatment. These results provide new molecular insights into

Correspondence: Changmeng Cai (changmeng.cai@umb.edu).

*W. H. and M. L. contributed equally to this work

AUTHOR CONTRIBUTIONS

C. Cai, S. Gao, W. Han, and M. Liu designed the study. W. Han, M. Liu, D. Han, M. Li, A. Toure, Z. Wang, A. Besschetnova, and S. Gao performed experiments and analyzed the results. W. Han, M. Liu, D. Han, S. Patalano, and J. Macoska performed deep sequencing analyses. C. Cai, W. Han, M. Liu, H. He, and S. Gao wrote the manuscript. All authors discussed the results and commented on the manuscript.

CONFLICT OF INTEREST

No potential conflicts of interest were disclosed.

The authors declare no potential conflicts of interest.

ACCESSION NUMBERS

The GEO accession number for the deposited ChIP-seq and RNA-seq data is GSE176404.

Rb activity in PCa progression and suggest that targeting LSD1 activity with small molecule inhibitors may be a potential treatment strategy to treat Rb-deficient CRPC.

Keywords

prostate cancer; androgen receptor; androgen deprivation therapy; transcriptional repression; DNA replication; KDM1A; LSD1; Retinoblastoma protein; Rb; E2F1; neuroendocrine prostate cancer

INTRODUCTION

The development of prostate cancer (PCa) depends on the activity of the androgen receptor (AR), a ligand-dependent nuclear transcription factor [1]. While PCa can be treated with androgen deprivation therapies (ADTs), including more aggressive AR signaling inhibition (ARSi) such as abiraterone and enzalutamide [2, 3], tumors inevitably relapse into the castration-resistant stage of PCa (called CRPC) [4]. Recent comprehensive genomic and transcriptomic studies indicated that ~10–15% of CRPC harbor biallelic deletion or loss-of-function alterations of *RB1* (encodes Retinoblastoma protein, Rb), which are significantly associated with poor patient survival [5–7]. Rb functions to repress the transcription activity of E2Fs by forming an Rb-E2F transcription repressor complex and the hyperphosphorylation of Rb during G1/S cell cycle transition results in its disassociation with E2Fs, thus inducing E2F-dependent transcriptional activation of DNA replication and cell cycle genes [8]. Notably, a subset of CRPC tumors (~15–20%) have similar features as small-cell neuroendocrine prostate cancer (NEPC or CRPC-NE), which is characterized by multiple genetic and epigenetic features, including low or absent AR expression, *RB1* deletions, *TP53* deletions/mutations, N-Myc overexpression, increased activity of EZH2, and the expression of neuroendocrine (NE) markers [9–12]. In particular, loss or inactivation of *RB1* is a major event found in 50–60% of CRPC-NE [5, 6, 9, 13, 14] and prior studies have reported that *RB1* loss not only facilitates the outgrowth of NE-like cells that have decreased AR signaling but together with *TP53* loss may contribute to the lineage reprogramming by stimulating expression of SOX2 [15, 16]. Importantly, this lineage plasticity appears to be driven by epigenetic changes that arise in a specific genomic context and EZH2 has been suggested as a master epigenetic regulator that promotes this process [15–17]. Clinically, it becomes urgent to identify actionable targets and develop novel strategies to treat these ARSi-resistant and Rb-deficient CRPC, including CRPC-NE.

In this study, we performed an integrated genomic analysis using two CRPC cell line models (C4–2 and VCaP) to distinguish the direct transcriptome changes versus the indirect adaptive effects in CRPC in response to *RB1* silencing. Despite that Rb-depletion similarly hyperactivates E2F signaling in both cell lines, Rb binding sites and targets are significantly different in VCaP cells versus C4–2 cells and *RB1* silencing in VCaP cells results in an increased expression of genes mediating hypoxia and other cancer-promoting pathways. As expected, we also demonstrated that Rb directly repressed genes are increased in CRPC-NE tumors. Significantly, we have revealed that Rb-deficient CRPC cells confer increased expression of a subset of genes that are activated by LSD1, a critical epigenetic regulator that is overexpressed in PCa [18, 19]. Interestingly, this activity is distinct to its canonical

repressor function as a member of the REST complex mediated by demethylating histone 3 lysine 4 (H3K4) [20, 21]. Mechanistically, we show that the hyperactivated E2F signaling requires this activity of LSD1 to maintain the chromatin binding of E2Fs. Moreover, we demonstrated that CRPC tumors with Rb inactivation are more sensitive to the LSD1 inhibitor treatment. Overall, our study provides new molecular insights into the activities of E2F, Rb, AR, and LSD1 in CRPC and suggests that LSD1 inhibition may be a potential therapeutic strategy to treat Rb-deficient CRPC.

RESULTS

Identification of Rb direct targets in CRPC models

To study the activity of Rb in CRPC, we generated a stable cell line expressing doxycycline-inducible lentiviral shRNA against *RB1* in C4–2 cells, a *PTEN*-null but Rb-proficient CRPC cell line derived from androgen-sensitive LNCaP line [22]. The protein expression of Rb was rapidly depleted by the doxycycline treatment (Figure 1A). As expected, *RB1* silencing in C4–2 cells significantly increased cell proliferation and decreased growth response to enzalutamide, a potent AR antagonist [3] (Figure 1B and C). To assess the direct transcriptomic changes by Rb inactivation, we first examined the chromatin binding of Rb in C4–2 cells by chromatin immunoprecipitation followed by high-throughput sequencing (ChIP-seq) of Rb. 9,146 high-confidence Rb binding peaks were identified, and these sites were highly enriched for the binding motifs of E2Fs (Figure 1D). In comparison with publicly available E2F1 ChIP-seq in C4–2 cells [23], we observed a large overlap (6,836) between Rb and E2F1 binding sites, suggesting that the majority of Rb binding sites are likely occupied by the Rb-E2F1 repressor complex (Figure 1E).

To study both acute and prolonged transcriptional effects of *RB1* silencing, we conducted RNA sequencing (RNA-seq) analysis using both short-term (3 days) and long-term (30 days) treatments of low-dose doxycycline (0.05 ug/ml). Binding and Expression Target Analysis (BETA, a target prediction analysis) [24] was then performed to globally determine the association of Rb binding with Rb-depletion induced/repressed gene expression and to identify potential Rb (Rb-E2F) directly regulated genes. As shown in Figure 1F, we found that the upregulated genes by either short-term or long-term Rb depletion (Rb-E2F repressed genes) were strongly associated with direct Rb chromatin binding while the downregulated genes were not associated with Rb binding, consistent with the canonical function of Rb as a member of the Rb-E2F transcription repressor complex. This analysis also suggests that the downregulation of genes by Rb depletion is primarily due to indirect effects. BETA also predicted and identified a subset of Rb directly regulated genes. Interestingly, while the short-term and long-term Rb-depletion may impact gene expression differently (Figure 1G and H), the subsequent Gene Set Enrichment Analysis (GSEA) indicated that the Rb directly repressed genes (by both short-term and long-term Rb depletion) were highly enriched for E2F targets (Figure 1I and J), consistent with previous findings [16, 25, 26]. These findings were also validated by a second C4–2-tet-shRB line using a different shRNA (Supplementary Figure S1A–C).

Next, we examined Rb activity in a second CRPC cell line, VCaP [27]. While both C4–2 and VCaP cell lines are AR positive CRPC models, each line has its own distinct

genomic background, such as differences in the status of *ERG* fusion, *PTEN* deletion, *AR* amplification and mutations, etc. Interestingly, VCaP cells also contain an R248W mutation of *TP53*, a possible gain-of-function mutation [28, 29]. It has been reported that a subset of *RB1*-loss CRPC tumors harbor *TP53* deletions or mutations [6, 14], and that the concurrent loss of *RB1* and *TP53* can promote the progression of CRPC [15, 16, 26]. Therefore, this *TP53* mutation in VCaP cells may potentially alter Rb activity. Nonetheless, we performed a similar study in VCaP cells and ChIP-seq analysis of Rb in VCaP cells revealed 17,026 binding sites that were enriched for E2F binding motifs (Figure 2A). While VCaP and C4–2 shared a significant portion of Rb binding sites (5,134), 70% of Rb binding sites in VCaP cells were unique (11,892) (Figure 2B and C; Supplementary Figure S2A and B). Next, we performed RNA-seq to identify Rb-E2F regulated genes in VCaP cells transfected with siRNAs against *RB1* versus non-target control (NTC) (Figure 2D). We then used BETA to determine the association of differential gene expression with Rb binding and predict Rb direct targets. As shown in Figure 2E, only the upregulated genes by Rb depletion were significantly associated with Rb binding sites, consistent with the finding in C4–2 cells. Interestingly, the VCaP-unique Rb binding sites were only associated with Rb targets in VCaP cells but not that in C4–2 cells (Supplementary Figure S3A and B), indicating that Rb-E2F cistrome may be altered in the VCaP line. Indeed, the direct targets of Rb (determined by BETA) were noticeably different in VCaP cells versus C4–2 cells (Figure 2F–I). While the predicted Rb direct targets were consistently enriched for E2F signaling in both models (such as regulating MCM DNA helicase genes and Fanconi Anemia Complementation Group genes), the Rb directly repressed genes differentially enriched for multiple pathways in VCaP versus C4–2 cells (Figure 2J and K). Notably, genes involved in p53 and hypoxia pathways (Supplementary Figure S4A; Figure 2L) were the predicted direct targets of Rb in VCaP cells but not in C4–2 cells, and recent studies have indicated that the upregulation of hypoxia may contribute to the development of CRPC-NE [12, 30–32]. In addition, the AR pathways also appeared to be enriched for Rb-repressed genes in VCaP but not C4–2 cells (Supplementary Figure S4B).

Rb directly repressed genes are upregulated in CRPC-NE

Through the analysis of the SU2C mCRPC dataset [6, 14], we found that the expression of activator E2Fs (E2F1–3) was increased in the CRPC with deep deletion of *RB1* (Figure 3A), while the expression of repressor E2Fs can be increased (E2F6–8) or decreased (E2F4) (Supplementary Figure S5). The increased expression of E2Fs appeared to be a direct transcriptional effect instead of an adaption effect since many of E2Fs were rapidly upregulated by Rb depletion (Figure 3B). Next, we developed several Rb-directly-regulated gene signatures from the BETA analysis of C4–2 or VCaP model (Supplementary Table S1) and then examined the expression of these Rb-target signatures in the SU2C mCRPC dataset. As shown in Figure 3C and D, the scores of Rb-directly-repressed gene signatures, determined by either short-term or long-term depletion of Rb in C4–2 cells, were significantly increased in *RB1*-loss CRPC. The Rb-activated gene targets were also downregulated in *RB1*-loss CRPC. On the contrary, the expression of Rb-repressed targets identified from VCaP cells was not significantly changed in the overall *RB1*-loss or *RB1*/*TP53*-loss CRPC (Figure 3E; Supplementary Figure S6A) or even in the subset of CRPC with concurrent *TP53* mutation and *RB1* deletion (Supplementary Figure S6B).

Furthermore, we also attempted to develop a common Rb-target signature. Since there were only a limited number of genes overlapped between the above C4–2 and VCaP Rb-target signatures, we decided to directly use the overlapping 49-gene (Rb-repressed) and 24-gene (Rb-activated) identified from Figure 2F as the common signatures (overlapping Rb directly regulated genes between C4–2-short-term and VCaP) and assessed their correlations with *RB1* status. As shown in Figure 3F, the common Rb-repressed genes were more significantly increased in *RB1*-loss CRPC than the C4–2 Rb-target signature. Therefore, we next assessed whether these Rb-target signatures can be used to predict patient outcomes. As shown in Figure 3G and H, the patients with higher scores of the C4–2 Rb-target signature or the common Rb-target signature (top 25%) were significantly associated with worse overall survival (from initiation of first-line ARSi). However, the difference appeared to be more significant for the common Rb-target signature (P=0.00014). We also compared this 49-gene Rb-target signature with *RB1* deletion status, *RB1* mRNA expression, and two published *RB1*-loss upregulated gene signatures for outcome prediction [26, 33]. As shown in Supplementary Figure S7A–D, only the status of *RB1* homozygous deletion (P=0.027) and one *RB1*-loss upregulated signature developed from LNCaP cells [26] (P=0.0092) were significant associated with poorer outcomes, but the P values were higher than using the common Rb direct targets (P=0.00014). Together, our data suggest a strong therapeutic potential of using this new Rb-target signature as a prognosis biomarker for CRPC progression.

Over 50% of CRPC-NE have *RB1* deep deletion (Figure 4A) and previously identified NE signature genes [34] are enriched in *RB1*-loss CRPC (Figure 4B). We next examined the expression of the identified Rb target signatures in this subset of CRPC. As shown in Figure 4C–E, the C4–2 Rb-target signatures or the common Rb-target signature (repressed-genes) were significantly upregulated in CRPC-NE. However, the Rb-target signature developed from the VCaP model was not increased in CRPC-NE (Supplementary Figure S8A). Previously, Ku and colleagues have established transgenic mouse models with $Pten^{-/-}$(SKO), $Pten^{-/-}/Rb1^{-/-}$ (DKO), and $Pten^{-/-}/Rb1^{-/-}/Trp53^{-/-}$ (TKO), and showed that DKO and TKO mice develop mixed luminal and NE tumors [15]. Therefore, we next determined whether our Rb-target gene signatures are increased in these *RB1*-loss models. Using published tumor RNA-seq data [15], we found that the C4–2 Rb-target signatures and the common Rb-target signature, but not the VCaP Rb-target signature, were significantly upregulated in DKO and TKO tumors (Figure 4F and G; Supplementary Figure S8B), suggesting that these Rb-repressed gene signatures may be directly relevant to the tumor progression and lineage plasticity *in vivo*. Moreover, the Rb repressed genes (by long-term Rb depletion in C4–2 cells) were highly enriched for the previously identified NE-upregulated gene set [9] (Figure 4H). However, only a few NE markers (SYP, ENO2, etc) were modestly increased by Rb depletion although Rb binding sites were found within these genes (Figure 4I and J; Supplementary Figure S9), suggesting that Rb inactivation alone is not sufficient to activate the NE program.

RB1 loss increases the expression of LSD1-activated genes

Epigenetic factors, such as EZH2 and SETD2, have been shown to play important roles in driving the progression of CRPC-NE [15, 35]. LSD1/KDM1A, a lysine-specific demethylase

that specifically demethylates mono- or di-methylated histone 3 lysine 4 (H3K4me1,2), together with CoREST and HDACs, are core components of REST complex, which functions to repress neuronal gene expression in non-neuronal cells [21, 31, 36]. Therefore, we next sought to determine whether LSD1 may play a role in mediating the development of CRPC-NE. Despite that LSD1 is overexpressed in CRPC adenocarcinoma and plays a critical role in promoting AR activity, its expression was further increased in *RB1*-loss CRPC and CRPC-NE from patient samples (Figure 5A and B). Interestingly, Rb depletion in C4–2 cells barely affected the expression of LSD1 and other components of the REST complex (Supplementary Figure S10A), suggesting that increased LSD1 expression in Rb-deficient CRPC patient samples may be an adaptive effect *in vivo*.

While the canonic function of LSD1 is a transcriptional repressor that silences gene expression through removing enhancer-associated H3K4me1,2, LSD1 can also function as a transcriptional activator through known and unknown mechanisms [18, 37–40]. Previous studies have shown that LSD1 promotes the progression of AR-high CRPC by stabilizing FOXA1 chromatin binding and AR-negative CRPC by a demethylase-independent activity mediated by ZNF217 [19, 40, 41]. Using our previously published dataset [19], we found that both activation and repression functions of LSD1 were strongly associated with LSD1 chromatin binding (Figure 5C), indicating that LSD1 can function as a direct activator at chromatin in PCa cells. Next, we examined whether Rb inactivation could affect both types of LSD1 activities. As shown in Figure 5D, Rb-depletion upregulated genes were significantly enriched for both LSD1 directly activated and repressed gene sets, suggesting that LSD1 activation function may be promoted and its repression function may be impaired by Rb depletion. Similar effects were also observed in the C4–2-tet-shRB cell line using a different shRNA (Supplementary Figure S10B). Moreover, this alteration of LSD1 activity is not associated with the change of LSD1 protein expression or the levels of total methylated H3K4 (Figure 5E). We next examined these LSD1 functions in the transgenic mouse tumors with *RB1* loss. As shown in Figure 5F, the score of the direct LSD1-activated gene signature was significantly increased in both DKO and TKO tumors, indicating that the activator function of LSD1 may be enhanced by *RB1*-loss in these models. In contrast, the LSD1-repressed gene signature was not significantly changed in *RB1*-loss tumors.

The sequencing results from both C4–2 and VCaP models (see Figure 1 and 2) indicate that hyperactivated E2F signaling, as expected, is the major direct consequence of Rb inactivation. Interestingly, previous studies have revealed that LSD1 may regulate E2F1 activity [38, 42]. Indeed, genes repressed by a small molecule LSD1 inhibitor (GSK2879552, LSD1-i) in LNCaP PCa cells were highly enriched for E2F signaling (Figure 5G), suggesting that E2F activity in PCa cells is mediated by LSD1. The histone demethylase activity of LSD1 requires its binding partner, CoREST, which is a core component of CoREST complex [21]. In C4–2 cells, we detected a very tight interaction between LSD1 and CoREST, which was not affected by Rb depletion (Figure 5H). Thus, we next examined whether E2F may interact with LSD1-CoREST complex. Surprisingly, while we confirmed a strong Rb-independent protein-protein interaction between LSD1 and E2F1 in C4–2 cells, we found that CoREST was not co-immunoprecipitated with E2F1 (Figure 5I). These data suggest that E2F may interact with a distinct CoREST-independent LSD1 complex.

A previous study has shown that LSD1 may demethylate E2F1 at K185 and this demethylation prevents the proteosome-dependent degradation of E2F1 protein in lung cancer cells [38]. However, it is not clear how LSD1 may regulate E2F1 signaling in PCa cells. To examine the effect of LSD1 on E2F1 chromatin binding in CRPC, we generated a V5-tagged E2F1-overexpressing (doxycycline-regulated) cell line, C4–2-tetE2F1. Interestingly, LSD1 inhibition did not increase the exogenous or endogenous E2F1 protein (Figure 5J), suggesting that LSD1 is unlikely to regulate E2F1 protein stability in PCa cells. Next, we performed ChIP-seq analysis of V5 in these stable cells treated with the LSD1 inhibitor and/or transfected with an siRNA pool against *RB1*. The V5 antibody used in the ChIP-seq analysis has been previously validated [40, 43] and the identified peaks were highly enriched for E2F motifs (Supplementary Figure S11A and B). Significantly, this treatment globally impaired the chromatin binding of E2F1 in C4–2 cells (Figure 5K), suggesting that LSD1 may function to stabilize E2F1 chromatin binding in PCa cells. More importantly, silencing *RB1* in these stable cells broadly increased global E2F1 binding, which can be markedly repressed by LSD1-i (Figure 5L and M). Interestingly, the repression of E2F1 binding also happened more rapidly in Rb-deficient cells than in Rb-proficient cells (Supplementary Figure S11C). Overall, these results suggest that Rb inactivation may promote an LSD1 activator function *in vitro* and *in vivo*, which can markedly enhance the chromatin binding of the E2F activator complex.

To further examine whether this effect may be mediated through the demethylation of E2F1-K185, we generated another cell line expressing a K185R mutant of E2F1 (Supplementary Figure S12A). LSD1-i increased the level of lysine-methylation on wildtype E2F1 but not K185R mutant, indicating that methylated-K185 is indeed the major substrate of LSD1 (Supplementary Figure S12B). However, despite modestly increasing H3K4me2 levels at E2F binding sites (Supplementary Figure S12C), LSD1 inhibition or silencing can still repress the chromatin binding of K185R mutant at several E2F1 binding sites (Supplementary Figure S12D–G). Moreover, ChIP-seq analyses showed that the global chromatin binding of E2F1-K185R mutant can be markedly repressed by LSD1-i even when Rb was ablated (Supplementary Figure S12H), suggesting that the effect of LSD1 on stabilizing E2F1 binding was unlikely mediated through K185 demethylation. Together, these results indicate that the increased E2F1 chromatin binding in Rb-deficient CRPC cells is dependent on LSD1 activity.

Targeting Rb-deficient CRPC with LSD1 inhibitor treatment

The above findings suggest that *RB1*-loss CRPC or CRPC-NE may be more sensitive to LSD1-i. Therefore, we next assessed the LSD1-i treatment in *RB1*-silenced C4–2 models *in vitro* and *in vivo*. We first examined the effect of LSD1-i on C4–2 cell proliferation. While the growth of parental C4–2 cells or uninduced C4–2-tet-shRB cells was not significantly affected by LSD1-i, the increased cell growth by *RB1* silencing can be repressed by LSD1-i (Supplementary Figure S13; Figure 6A). Moreover, LSD1-i appeared to resensitize Rb-depleted C4–2 cells to enzalutamide treatment (Figure 6B). We then performed RNA-seq analysis to determine the global transcriptomic effect of LSD1-i in C4–2 cells (Supplementary Figure S14A). As shown in Figure 6C and Supplementary Figure S14B, LSD1-i repressed genes were enriched for E2F signaling and G2/M cell cycle

regulation, consistent with the findings in LNCaP cells (see Figure 5G). Importantly, the enrichment of E2F signaling appeared to be increased in Rb-depleted cells. In addition, Myc signaling (MYC_TARGET_V2) and oxidative phosphorylation pathways were both found enriched in Rb-depleted cells but not in Rb-proficient cells. This broad repression activity of LSD1-i on these pathways was confirmed by examining the effect on expression levels of related genes (Figure 6D; Supplementary Figure S14C). The effect of LSD1-i on the expression of several E2F-regulated genes was further validated by qRT-PCR (Figure 6E). Interestingly, the canonical AR targets were not repressed by LSD1-i (Supplementary Figure S14D). The relative resistance of AR signaling to LSD1-i in the C4–2 model in comparison to the much stronger response previously found in the CWR22-RV1 CRPC model [40] may be due to the significantly lower expression of FOXA1 in C4–2 cells in comparison with other AR-positive cell lines (Supplementary Figure S14E).

We then established CRPC xenografts using the C4–2-tet-shRB cell line and examined how *RB1* silencing impacts the efficacy of LSD1-i. Consistent with the *in vitro* cell proliferation results, while xenograft tumors with Rb expression did not appear to respond to LSD1-i, tumors with Rb depletion were noticeably repressed by the LSD1 inhibitor treatment (Figure 6F and G), suggesting that *RB1*-loss CRPC or CRPC-NE may be more sensitive to the LSD1-i treatment. Consistent with the effect on tumor growth, LSD1-i significantly decreased the expression of E2F transcriptional targets in *RB1*-silenced tumors but not in *RB1*-positive tumors (Figure 6H). Moreover, the expression of AR targets was not significantly repressed by LSD1-i (Supplementary Figure S15). Together, these data indicate that the hyperactivated E2F signaling in *RB1*-loss CRPC can be targeted by LSD1 inhibitor treatment.

DISCUSSION

Biallelic deletion of *RB1* is one of the most frequent genetic alterations of CRPC-NE but it can also happen in the AR-active adenocarcinoma subtype of CRPC [7, 26]. Our data show that *RB1* loss induces hyperactivated E2F signaling by increasing the expression of E2F transcription activators and by activating the E2F-mediated transcription program in multiple CRPC models. Interestingly, while our combined analyses of ChIP-seq and RNA-seq in *RB1*-silenced C4–2 cells did not reveal any major enrichment for additional pathways mediated by Rb, the study using the VCaP CRPC model suggests altered Rb chromatin binding and activities in repressing p53, hypoxia, and interferon pathways (see Figure 2). In particular, increased hypoxia signaling has been reported as a hallmark of CRPC-NE and is possibly regulated by FOXA2 and ONECUT2 [32, 44]. Therefore, our data suggest that the differences of genomic background in PCa cells may strongly influence the Rb-E2F transcription repression program. Interestingly, VCaP cells contain a possible gain-of-function mutation of *TP53*, and this type of *TP53* mutation may have distinct functions versus *TP53* deletion in altering Rb-E2F activity and mediating CRPC progression. Future studies are required to determine whether the reprogrammed Rb-E2F signaling in VCaP model is due to this *TP53* mutation or other genomic differences.

Another important finding is that we did not observe an apparent change of linage plasticity in any of our *RB1*-silencing models. This is different to the findings using

AR-overexpressing LNCaP or transgenic mouse models with concurrent silencing of *RB1* and *TP53*, which induces SOX2 activity and dramatically increases the expression of NE markers [15, 16], but is consistent with a recent study using LNCaP cells with CRISPR/Cas9 mediated *RB1*/*TP53* silencing [26]. Therefore, our data suggest that *RB1* loss, which may activate a program that is required for the establishment of CRPC-NE, is insufficient to directly drive NE differentiation, and that the tumor progression to CRPC-NE may require further adaptation and epigenetic reprogramming.

In this study, we have also developed a 49-gene common Rb-target signature as a robust readout of Rb repression activity in patient samples. By analyzing SU2C dataset, we demonstrated that CRPC tumors carrying *RB1* deep deletion had significantly higher scores of this signature, and that patients with higher scores were strongly associated with the worse overall survival. These data indicate a strong correlation of Rb activity and treatment outcomes in CRPC and this common Rb-target signature may have a therapeutic potential to be developed as a biomarker to predict Rb deficiency and the aggressiveness of CRPC after ARSi treatments.

Previous studies indicated that epigenetic changes are the essential factors to drive NEPC progression [12]. EZH2 has been suggested as such a factor to regulate the linage change of tumor cells and the treatment of EZH2 inhibitor can resensitize PCa tumors to aggressive ARSi treatments [15–17]. In this study, we have identified LSD1, as another possible critical epigenetic factor in CRPC-NE. This finding is quite surprising since LSD1 is a well-known neuronal repressor [20, 21] and can also function as a critical AR coactivator in promoting the development of adenocarcinoma PCa through multiple mechanisms, including demethylating histones residues other than H3K4 or non-histone proteins [18, 19, 40, 45, 46]. Our recent study also suggests that LSD1 can enhance AR chromatin recruitment by demethylating its pioneer factor FOXA1 and thus stabilizing its chromatin binding [40]. However, examining the CRPC patient cohort and murine NEPC models, we found that LSD1 expression is further increased in CRPC with *RB1* loss or in CRPC-NE, indicating that LSD1 may play a distinct function in those CRPC subtypes (see Figure 5). Importantly, our data show that *RB1* loss can increase the expression of genes that are associated with a noncanonical activator function of LSD1 but not its classic repressor function which is commonly associated with its H3K4 demethylase activity. One possible activator function of LSD1 would be regulating the AR activity through enhancing FOXA1 binding [40]. However, the expression of those AR canonical targets was not repressed by LSD1 inhibition (see Supplementary Figure S14 and 15), suggesting that the increased expression of LSD1-activated genes by *RB1* loss is unlikely associated with the enhancement of AR signaling.

Since LSD1 activity has been linked to E2F and Rb in cancer cells [38, 39, 42], we proposed a model that LSD1 may be critical for enhancing E2F signaling, particularly when Rb is depleted and E2F signaling is hyperactivated. Previously, LSD1 has been shown to directly demethylate E2F1 at K185 and this demethylation stabilizes E2F1 protein expression in p53-deficient tumors [38]. In our study, we found that LSD1 inhibition can rapidly and dramatically repress the E2F1 chromatin binding in Rb-deficient CRPC cells without affecting E2F1 protein expression (see Figure 5). While we confirmed that LSD1

can demethylate E2F1-K185 in PCa cells, the chromatin binding of E2F1-K185R mutant can still be markedly repressed by LSD1 inhibition, suggesting that K185-demethylation is unlikely the mechanism mediating LSD1-enhanced E2F1 chromatin binding. Using co-immunoprecipitation assays, we detected a strong interaction between E2F1 and LSD1 in C4–2 cells. However, it appears that E2F1 may interact with a distinct LSD1 complex that does not contain its well-known partner, CoREST. These data suggest that LSD1 may regulate E2F chromatin binding through demethylating other histone or non-histone proteins that are critical for E2F chromatin binding, or indirect mechanisms such as epigenetic reprogramming. Another possible mechanism that may contribute to LSD1 activator activity in NEPC is increased expression of neuronal LSD1 splice variant, LSD1+8a, which does not interact with CoREST and therefore cannot effectively demethylate H3K4 [47]. LSD1+8a function has been recently characterized in LNCaP cells [48] but its chromatin activity in NEPC models remains to be determined. Nonetheless, it is of importance to decipher this molecular mechanism in future studies. Overall, we propose a model that LSD1 may function as a coactivator of E2F1 by interacting with E2F1 and thus enhancing E2F1 chromatin binding in PCa cells. In Rb-proficient cells, E2F1 transcription activity was repressed by forming the complex with Rb and thus was less dependent on LSD1-mediated E2F1 chromatin binding. However, Rb-deficiency can unleash the chromatin binding and activity of E2F1, which are now highly dependent on the LSD1-enhanced E2F1 chromatin binding, and thus make Rb-deficient PCa cells vulnerable to LSD1 downregulation or inhibition.

LSD1 inhibitors have been tested in clinical trials of leukemia and small cell lung cancer, as well as other solid tumors, and several of them (ORY1001 and INCB059872) have entered phase II trials [49]. A previous study also demonstrated the efficacy of a structurally distinct LSD1 inhibitor (SP2509) in treating PC-3 derived xenograft, an NE-like CRPC model [41]. Our *in vivo* study using an LSD1 inhibitor (GSK2879552) in C4–2 derived xenograft models suggests that Rb-deficient CRPC tumors may be more vulnerable to LSD1-i. Additional preclinical studies assessing different LSD1 inhibitors in *RB1*-loss CRPC models (both adenocarcinoma and NE subtypes) are clearly required to demonstrate the full potential of LSD1-i therapy in treating these PCa subtypes. Overall, our study provides a strong rationale for testing LSD1 inhibitors in Rb-deficient CRPC or CRPC-NE and the findings will have an impact on the therapeutic development of targeted therapies in treating these lethal and highly aggressive CRPC subtypes.

MATERIALS AND METHODS

Cell culture, transfection, and establishment of stable cell lines:

C4–2 and VCaP cell lines were obtained from American Type Culture Collection (ATCC). All cell lines were checked for mycoplasma using MycoAlert Mycoplasma Detection Kit (Lonza) and authenticated using short tandem repeat (STR) profiling. VCaP cells were maintained in DMEM medium with 10% fetal bovine serum (FBS). C4–2 cells were maintained in RPMI 1640 medium with reduced steroid hormone [8% charcoal-stripped FBS (CSS) plus 2% regular FBS]. For transient transfection of siRNA, cells were transfected with 20nM of siRNA (non-target control or siRB1) for 2d. siRNAs were predesigned and

obtained from Dharmacon RNAi Technologies (ON-TARGETplus). For stable infection of lentiviral shRNA, tetracycline-inducible shRNA constructs (pTRIPZ) against non-target control or *RB1* (obtained from Dharmacon) were used to assemble lentivirus, and then C4–2 cells were infected with these viruses and selected by puromycin (1μg/ml). All stable cell lines were maintained in culture medium with tetracycline-free FBS.

Cell proliferation assay:

Cells were collected and trypsinized to examine the number of cells and viability by using Muse® Count & Viability Kit 200X following manufacture protocol using Guava Muse Cell Analyzer.

Immunoprecipitation and immunoblotting:

For immunoprecipitation (IP), cells were lysed in Triton lysis buffer supplemented with protein inhibitor cocktails (Thermo Fisher Scientific), followed by a brief sonication, and then lysates were immunoprecipitated with anti-E2F1 (Abcam), anti-LSD1 (Abcam), or anti-CoREST (Abcam) antibodies. For immunoblotting, proteins were separated on 4–15% SDS gradient gels (Bio-Rad), transferred to nitrocellulose membranes (Bio-Rad), and then probed with primary antibodies, including anti-Rb (Cell Signaling), anti-tubulin (Abcam), anti-LSD1 (Abcam), anti-CoREST (Abcam), anti-E2F1 (Cell Signaling), anti-GAPDH (Abcam), anti-V5 (Abcam), anti-H3 (Abcam) and anti-FOXA1 (Abcam).

Chromatin immunoprecipitation sequencing (ChIP-seq):

For the preparation of ChIP-seq, cells were fixed with 1% formaldehyde and then lysed by the ChIP lysis buffer. Chromatin was then sheared to ~300bp fragments using Bioruptor Sonicator (Diagenode). Immunoprecipitation was carried out using anti-Rb antibody (Cell signaling and BD Pharmingen) or anti-V5 antibody (Thermo Scientific). DNA libraries were constructed using the SMARTer ThruPLEX DNA-Seq Prep Kit (Takara Bio USA). Next-generation sequencing (51nt, single-end) was performed using Illumina HiSeq2500. ChIP-sequencing reads were mapped to the hg19 human reference genome and peak calling was performed using MACS2 (version 2.1.0) [50].

Quantitative RT-PCR and RNA-sequencing (RNA-seq):

RNA from cell lines was extracted with TRIzol reagent (Invitrogen). RNA from tumor tissue samples, which were homogenized by TissueLyser LT (Qiagen), was extracted using RNeasy Kit (Qiagen). Quantitative Reverse Transcription PCR (qRT-PCR) was performed using Fast 1-step Mix (Thermo Fisher Scientific). All qRT-PCR data were normalized with an internal control GAPDH and quantitated by calculating ΔΔCt. All Taqman primers and probes were predesigned and obtained from Thermo Fisher Scientific. For RNA-seq, library preparation was performed using TruSeq Strnd Total RNA LT (Illumina). Next-generation sequencing (51nt, single-end) was performed using Illumina HiSeq2500. Transcriptome-sequencing reads were aligned to the hg19 human reference genome. Differential gene expression was analyzed by using R package limma (3.40.6) [51].

Xenograft study:

All animal experiments were approved by the University of Massachusetts Boston Institutional Animal Care and Use Committee and were conducted following institutional and national (USA) guidelines. To establish the xenograft tumors, C4–2-tet-shRB cells mixed with Matrigel (BD Biosciences) were subcutaneously injected (2×10^6 cells per injection) on flanks of castrated male SCID mice (~6-week old, Taconic). Xenograft tumors were further passaged in castrated mice. To silencing Rb, mice were fed with doxycycline supplemented food and drinking water. Tumor length (L) and width (W) were measured by caliper every other day during the treatment period and tumor volumes were calculated (L × W2/2). The tumor cell proliferation was examined by immunohistochemistry staining of Ki67 (anti-Ki67: ab16667 from Abcam, performed by iHisto).

Statistical analysis:

Data in bar graphs represent mean±SD of at least 3 biological repeats. Statistical analysis was performed using unpaired two-tailed Student's *t*-test by comparing treatment versus vehicle or otherwise as indicated. *P*-value<0.05 (*) was considered to be statistically significant. The results for immunoblotting are representative of at least three experiments. Boxplots of signature scores and gene expression were compared using the Wilcoxon test for comparison between two groups of samples. Boxplots of enriched hallmark gene sets were compared using paired *t*-test. The difference in tumor growth (n=6) was determined using two-way ANOVA. These tests were parametric and based on the assumption of normal distribution and equal variance across all experimental groups. All statistical analyses and visualization were performed with R (version 3.6.0) unless otherwise specified.

Supplementary Material

Refer to Web version on PubMed Central for supplementary material.

ACKNOWLEDGMENTS

This work is supported by grants from NIH (R00 CA166507 and R01 CA211350 to C.C., U54 CA156734 to J.A.M), DOD (W81XWH-16-1-0445, W81XWH-19-1-0361, and W81XWH-21-1-0267 to C.C., W81XWH-19-1-0777 to S.G.), CIHR (142246, 152863, 152864, and 159567 to H.H.H.), and Terry Fox Frontiers Program Project Grants (1090 P3 to H.H.H.). M. Liu was supported by the graduate fellowship from the Integrative Biosciences Program at the University of Massachusetts Boston. W. Han and Z. Wang were supported by CSM (College of Science and Mathematics) Dean's Doctoral Research Fellowship from the University of Massachusetts Boston. H.H.H. holds Joey and Toby Tanenbaum Brazilian Ball Chair in Prostate Cancer.

REFERENCES

1. Watson PA, Arora VK, Sawyers CL. Emerging mechanisms of resistance to androgen receptor inhibitors in prostate cancer. Nat Rev Cancer 2015; 15: 701–711. [PubMed: 26563462]
2. de Bono JS, Logothetis CJ, Molina A, Fizazi K, North S, Chu L et al. Abiraterone and increased survival in metastatic prostate cancer. N Engl J Med 2011; 364: 1995–2005. [PubMed: 21612468]
3. Scher HI, Fizazi K, Saad F, Taplin ME, Sternberg CN, Miller K et al. Increased survival with enzalutamide in prostate cancer after chemotherapy. N Engl J Med 2012; 367: 1187–1197. [PubMed: 22894553]
4. Yuan X, Cai C, Chen S, Chen S, Yu Z, Balk SP. Androgen receptor functions in castration-resistant prostate cancer and mechanisms of resistance to new agents targeting the androgen axis. Oncogene 2014; 33: 2815–2825. [PubMed: 23752196]

5. Quigley DA, Dang HX, Zhao SG, Lloyd P, Aggarwal R, Alumkal JJ et al. Genomic Hallmarks and Structural Variation in Metastatic Prostate Cancer. Cell 2018; 175: 889. [PubMed: 30340047]
6. Abida W, Cyrta J, Heller G, Prandi D, Armenia J, Coleman I et al. Genomic correlates of clinical outcome in advanced prostate cancer. Proc Natl Acad Sci U S A 2019; 116: 11428–11436. [PubMed: 31061129]
7. Mateo J, Seed G, Bertan C, Rescigno P, Dolling D, Figueiredo I et al. Genomics of lethal prostate cancer at diagnosis and castration resistance. J Clin Invest 2020; 130: 1743–1751. [PubMed: 31874108]
8. Dick FA, Rubin SM. Molecular mechanisms underlying RB protein function. Nature reviews Molecular cell biology (Research Support, N.I.H., Extramural Research Support, Non-U.S. Gov't Review) 2013; 14: 297–306. [PubMed: 23594950]
9. Beltran H, Rickman DS, Park K, Chae SS, Sboner A, MacDonald TY et al. Molecular characterization of neuroendocrine prostate cancer and identification of new drug targets. Cancer Discov 2011; 1: 487–495. [PubMed: 22389870]
10. Beltran H, Hruszkewycz A, Scher HI, Hildesheim J, Isaacs J, Yu EY et al. The Role of Lineage Plasticity in Prostate Cancer Therapy Resistance. Clin Cancer Res 2019; 25: 6916–6924. [PubMed: 31363002]
11. Conteduca V, Oromendia C, Eng KW, Bareja R, Sigouros M, Molina A et al. Clinical features of neuroendocrine prostate cancer. Eur J Cancer 2019; 121: 7–18. [PubMed: 31525487]
12. Rubin MA, Bristow RG, Thienger PD, Dive C, Imielinski M. Impact of Lineage Plasticity to and from a Neuroendocrine Phenotype on Progression and Response in Prostate and Lung Cancers. Mol Cell 2020; 80: 562–577. [PubMed: 33217316]
13. Grasso CS, Wu YM, Robinson DR, Cao X, Dhanasekaran SM, Khan AP et al. The mutational landscape of lethal castration-resistant prostate cancer. Nature 2012; 487: 239–243. [PubMed: 22722839]
14. Robinson D, Van Allen EM, Wu YM, Schultz N, Lonigro RJ, Mosquera JM et al. Integrative clinical genomics of advanced prostate cancer. Cell 2015; 161: 1215–1228. [PubMed: 26000489]
15. Ku SY, Rosario S, Wang Y, Mu P, Seshadri M, Goodrich ZW et al. Rb1 and Trp53 cooperate to suppress prostate cancer lineage plasticity, metastasis, and antiandrogen resistance. Science 2017; 355: 78–83. [PubMed: 28059767]
16. Mu P, Zhang Z, Benelli M, Karthaus WR, Hoover E, Chen CC et al. SOX2 promotes lineage plasticity and antiandrogen resistance in TP53- and RB1-deficient prostate cancer. Science 2017; 355: 84–88. [PubMed: 28059768]
17. Berger A, Brady NJ, Bareja R, Robinson B, Conteduca V, Augello MA et al. N-Myc-mediated epigenetic reprogramming drives lineage plasticity in advanced prostate cancer. J Clin Invest 2019; 129: 3924–3940. [PubMed: 31260412]
18. Metzger E, Wissmann M, Yin N, Muller JM, Schneider R, Peters AH et al. LSD1 demethylates repressive histone marks to promote androgen-receptor-dependent transcription. Nature 2005; 437: 436–439. [PubMed: 16079795]
19. Cai C, He HH, Gao S, Chen S, Yu Z, Gao Y et al. Lysine-specific demethylase 1 has dual functions as a major regulator of androgen receptor transcriptional activity. Cell Rep 2014; 9: 1618–1627. [PubMed: 25482560]
20. Shi Y, Lan F, Matson C, Mulligan P, Whetstine JR, Cole PA et al. Histone demethylation mediated by the nuclear amine oxidase homolog LSD1. Cell 2004; 119: 941–953. [PubMed: 15620353]
21. Shi YJ, Matson C, Lan F, Iwase S, Baba T, Shi Y. Regulation of LSD1 histone demethylase activity by its associated factors. Mol Cell 2005; 19: 857–864. [PubMed: 16140033]
22. Pfitzenmaier J, Quinn JE, Odman AM, Zhang J, Keller ET, Vessella RL et al. Characterization of C4–2 prostate cancer bone metastases and their response to castration. J Bone Miner Res 2003; 18: 1882–1888. [PubMed: 14584899]
23. Mandigo AC, Yuan W, Xu K, Gallagher P, Pang A, Guan YF et al. RB/E2F1 as a master regulator of cancer cell metabolism in advanced disease. Cancer Discov 2021.
24. Wang S, Sun H, Ma J, Zang C, Wang C, Wang J et al. Target analysis by integration of transcriptome and ChIP-seq data with BETA. Nature protocols (Research Support, N.I.H., Extramural Research Support, Non-U.S. Gov't) 2013; 8: 2502–2515. [PubMed: 24263090]

25. McNair C, Xu K, Mandigo AC, Benelli M, Leiby B, Rodrigues D et al. Differential impact of RB status on E2F1 reprogramming in human cancer. J Clin Invest 2018; 128: 341–358. [PubMed: 29202480]
26. Nyquist MD, Corella A, Coleman I, De Sarkar N, Kaipainen A, Ha G et al. Combined TP53 and RB1 Loss Promotes Prostate Cancer Resistance to a Spectrum of Therapeutics and Confers Vulnerability to Replication Stress. Cell Rep 2020; 31: 107669. [PubMed: 32460015]
27. Korenchuk S, Lehr JE, L MC, Lee YG, Whitney S, Vessella R et al. VCaP, a cell-based model system of human prostate cancer. In Vivo 2001; 15: 163–168. [PubMed: 11317522]
28. Song H, Hollstein M, Xu Y. p53 gain-of-function cancer mutants induce genetic instability by inactivating ATM. Nat Cell Biol 2007; 9: 573–580. [PubMed: 17417627]
29. Zhao Y, Ding L, Wang D, Ye Z, He Y, Ma L et al. EZH2 cooperates with gain-of-function p53 mutants to promote cancer growth and metastasis. The EMBO journal 2019; 38.
30. Danza G, Di Serio C, Rosati F, Lonetto G, Sturli N, Kacer D et al. Notch signaling modulates hypoxia-induced neuroendocrine differentiation of human prostate cancer cells. Mol Cancer Res 2012; 10: 230–238. [PubMed: 22172337]
31. Lin TP, Chang YT, Lee SY, Campbell M, Wang TC, Shen SH et al. REST reduction is essential for hypoxia-induced neuroendocrine differentiation of prostate cancer cells by activating autophagy signaling. Oncotarget 2016; 7: 26137–26151. [PubMed: 27034167]
32. Guo H, Ci X, Ahmed M, Hua JT, Soares F, Lin D et al. ONECUT2 is a driver of neuroendocrine prostate cancer. Nat Commun 2019; 10: 278. [PubMed: 30655535]
33. Chen WS, Alshalalfa M, Zhao SG, Liu Y, Mahal BA, Quigley DA et al. Novel RB1-Loss Transcriptomic Signature Is Associated with Poor Clinical Outcomes across Cancer Types. Clin Cancer Res 2019; 25: 4290–4299. [PubMed: 31010837]
34. Beltran H, Prandi D, Mosquera JM, Benelli M, Puca L, Cyrta J et al. Divergent clonal evolution of castration-resistant neuroendocrine prostate cancer. Nat Med 2016; 22: 298–305. [PubMed: 26855148]
35. Yuan H, Han Y, Wang X, Li N, Liu Q, Yin Y et al. SETD2 Restricts Prostate Cancer Metastasis by Integrating EZH2 and AMPK Signaling Pathways. Cancer Cell 2020; 38: 350–365 e357. [PubMed: 32619406]
36. Zhang X, Coleman IM, Brown LG, True LD, Kollath L, Lucas JM et al. SRRM4 Expression and the Loss of REST Activity May Promote the Emergence of the Neuroendocrine Phenotype in Castration-Resistant Prostate Cancer. Clin Cancer Res 2015; 21: 4698–4708. [PubMed: 26071481]
37. Huang J, Sengupta R, Espejo AB, Lee MG, Dorsey JA, Richter M et al. p53 is regulated by the lysine demethylase LSD1. Nature 2007; 449: 105–108. [PubMed: 17805299]
38. Kontaki H, Talianidis I. Lysine methylation regulates E2F1-induced cell death. Mol Cell 2010; 39: 152–160. [PubMed: 20603083]
39. Cho HS, Suzuki T, Dohmae N, Hayami S, Unoki M, Yoshimatsu M et al. Demethylation of RB regulator MYPT1 by histone demethylase LSD1 promotes cell cycle progression in cancer cells. Cancer Res 2011; 71: 655–660. [PubMed: 21115810]
40. Gao S, Chen S, Han D, Wang Z, Li M, Han W et al. Chromatin binding of FOXA1 is promoted by LSD1-mediated demethylation in prostate cancer. Nat Genet 2020.
41. Sehrawat A, Gao L, Wang Y, Bankhead A 3rd, McWeeney SK, King CJ et al. LSD1 activates a lethal prostate cancer gene network independently of its demethylase function. Proc Natl Acad Sci U S A 2018; 115: E4179–E4188. [PubMed: 29581250]
42. He Y, Zhao Y, Wang L, Bohrer LR, Pan Y, Wang L et al. LSD1 promotes S-phase entry and tumorigenesis via chromatin co-occupation with E2F1 and selective H3K9 demethylation. Oncogene 2018; 37: 534–543. [PubMed: 28991226]
43. Gao S, Chen S, Han D, Barrett D, Han W, Ahmed M et al. Forkhead domain mutations in FOXA1 drive prostate cancer progression. Cell Res 2019; 29: 770–772. [PubMed: 31324883]
44. Qi J, Nakayama K, Cardiff RD, Borowsky AD, Kaul K, Williams R et al. Siah2-dependent concerted activity of HIF and FoxA2 regulates formation of neuroendocrine phenotype and neuroendocrine prostate tumors. Cancer Cell 2010; 18: 23–38. [PubMed: 20609350]

45. Metzger E, Yin N, Wissmann M, Kunowska N, Fischer K, Friedrichs N et al. Phosphorylation of histone H3 at threonine 11 establishes a novel chromatin mark for transcriptional regulation. Nat Cell Biol 2008; 10: 53–60. [PubMed: 18066052]

46. Metzger E, Imhof A, Patel D, Kahl P, Hoffmeyer K, Friedrichs N et al. Phosphorylation of histone H3T6 by PKCbeta(I) controls demethylation at histone H3K4. Nature 2010; 464: 792–796. [PubMed: 20228790]

47. Laurent B, Ruitu L, Murn J, Hempel K, Ferrao R, Xiang Y et al. A specific LSD1/KDM1A isoform regulates neuronal differentiation through H3K9 demethylation. Mol Cell 2015; 57: 957–970. [PubMed: 25684206]

48. Coleman DJ, Sampson DA, Sehrawat A, Kumaraswamy A, Sun D, Wang Y et al. Alternative splicing of LSD1+8a in neuroendocrine prostate cancer is mediated by SRRM4. Neoplasia 2020; 22: 253–262. [PubMed: 32403054]

49. Fang Y, Liao G, Yu B. LSD1/KDM1A inhibitors in clinical trials: advances and prospects. J Hematol Oncol 2019; 12: 129. [PubMed: 31801559]

50. Zhang Y, Liu T, Meyer CA, Eeckhoute J, Johnson DS, Bernstein BE et al. Model-based analysis of ChIP-Seq (MACS). Genome Biol 2008; 9: R137. [PubMed: 18798982]

51. Ritchie ME, Phipson B, Wu D, Hu Y, Law CW, Shi W et al. limma powers differential expression analyses for RNA-sequencing and microarray studies. Nucleic Acids Res 2015; 43: e47. [PubMed: 25605792]

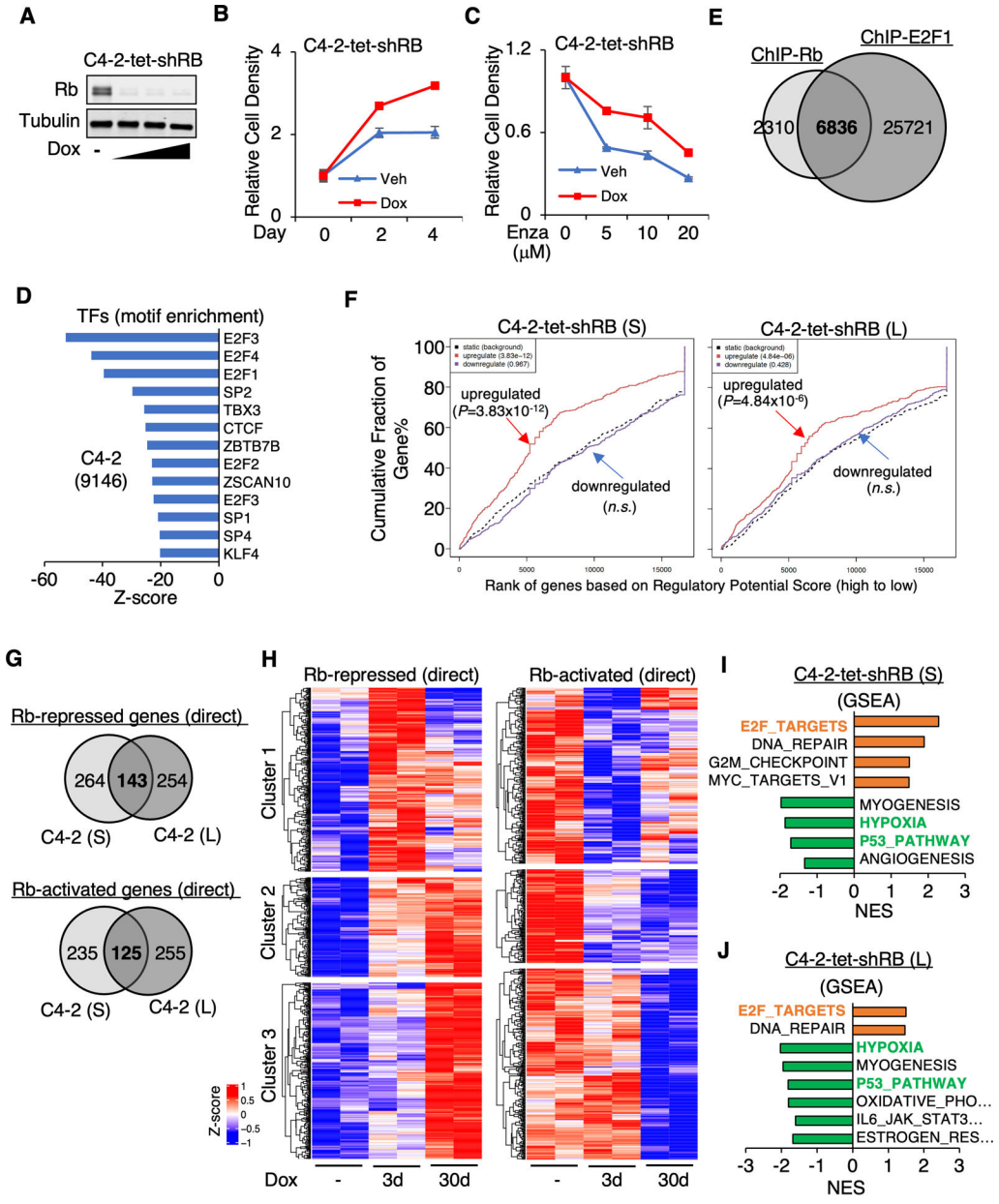

Figure 1. Identification of Rb directly regulated genes in C4–2 CRPC cells

(**A**) Immunoblotting for Rb in the doxycycline (dox, 0–0.25 μg/ml)-treated C4–2-tet-shRB cells (C4–2 cells stably infected by doxycycline-inducible lentiviral shRNA against *RB1*). (**B**) Proliferation assay for C4–2-tet-shRB cells treated with or without doxycycline (0.05 μg/ml). (**C**) Proliferation assay for C4–2-tet-shRB cells treated with 0–20μM of enzalutamide for 6 days (d) and with or without doxycycline. (**D**) Motif enrichment analysis of Rb ChIP-seq in C4–2 cells. (**E**) The Venn diagram for ChIP-Rb and ChIP-E2F1 peaks in C4–2 cells. (**F**) Binding and Expression Target Analysis (BETA) for the association of Rb binding sites with the expression of Rb-depletion up/downregulated genes after 3d (short-term, S) or 30d (long-term, L) of doxycycline treatment in C4–2-tet-shRB cells (data obtained from RNA-seq). (**G**) Venn diagrams for the predicted Rb direct targets determined

by short-term (3d, S) or long-term (30d, L) Rb depletion in C4–2-tet-shRB cells (using BETA). (**H**) Heatmap view for the predicted Rb direct targets (repressed/activated genes) determined by BETA (both short-term and long-term). (**I**, **J**) Gene Set Enrichment Analyses (GSEA) showing the significantly enriched hallmark gene sets (cutoff: $P<0.05$, ranked by normalized enrichment score) for short-term (I) or long-term (J) Rb directly regulated genes in C4–2-tet-shRB.

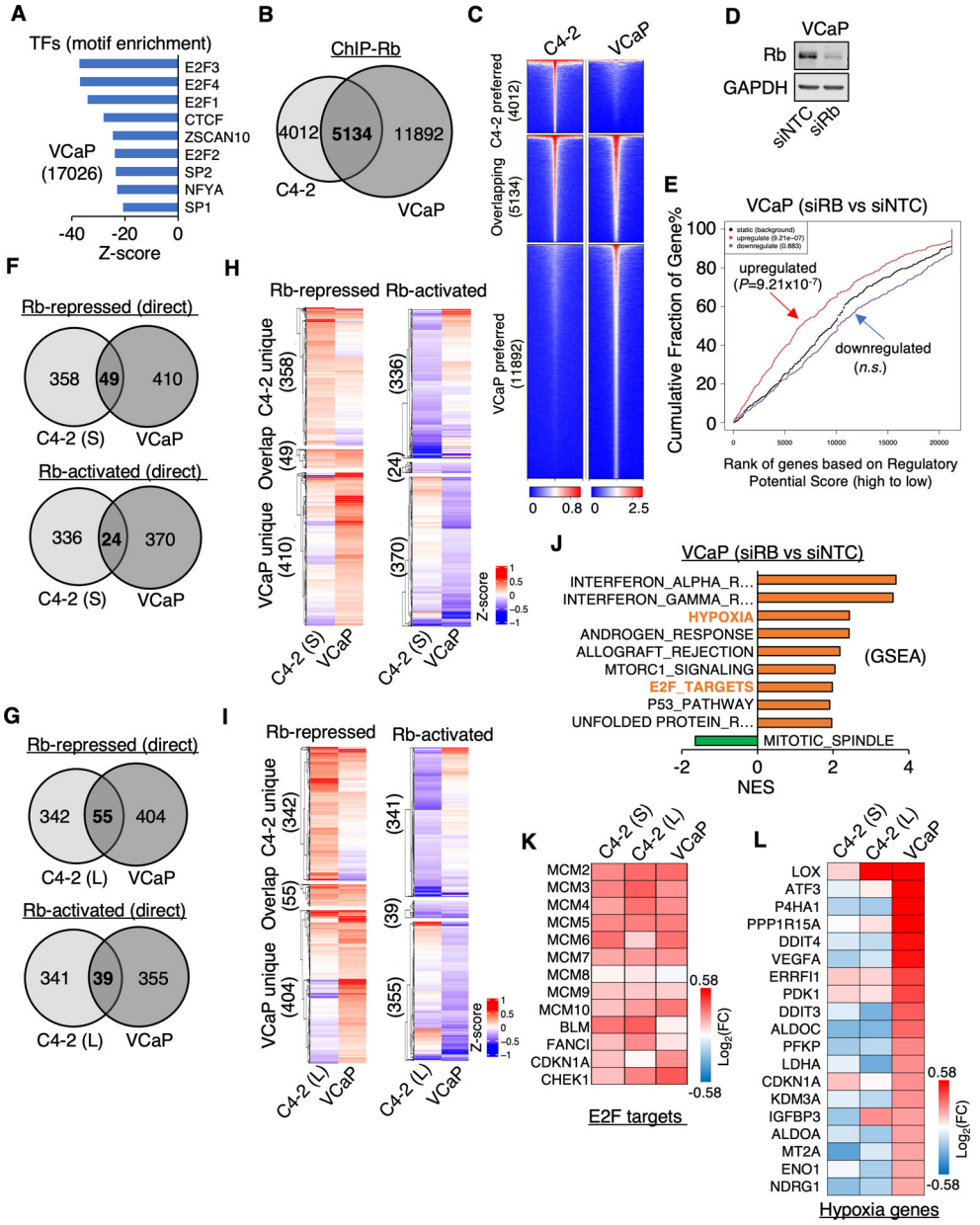

Figure 2. Rb directly represses distinct gene subsets in VCaP cells

(**A**) Motif enrichment analysis for Rb ChIP-seq in VCaP cells. (**B**) The Venn diagram for ChIP-Rb peaks in C4–2 and VCaP cells. (**C**) Heatmap view for ChIP-seq signal intensity of Rb in C4–2 and VCaP cells at clustered binding sites (C4–2 unique, C4–2/VCaP overlapping, and VCaP unique). (**D**) Immunoblotting for Rb in VCaP cells transfected with siNTC or siRB. (**E**) BETA for the association of Rb binding sites with the expression of Rb-depletion up/downregulated genes in VCaP model. (**F**, **G**) Venn diagrams for Rb directly regulated genes determined from BETA in C4–2-tet-shRB cells with short-term (F) or long-term (G) Rb-depletion versus VCaP cells. (**H**, **I**) Heatmap views for the expression of Rb direct targets in C4–2-tet-shRB cells with short-term (H) or long-term (I) Rb-depletion and VCaP cells (three clusters: C4–2 unique, overlapping, and VCaP unique targets). (**J**)

GSEA for the significantly enriched hallmark gene sets (cutoff: $P<0.05$) for Rb directly repressed/activated genes in VCaP cells. (**K**, **L**) Heatmap view for a panel of known E2F targets (K) or hypoxia genes (L) in C4–2-tet-shRB (short-term and long-term) and VCaP cells.

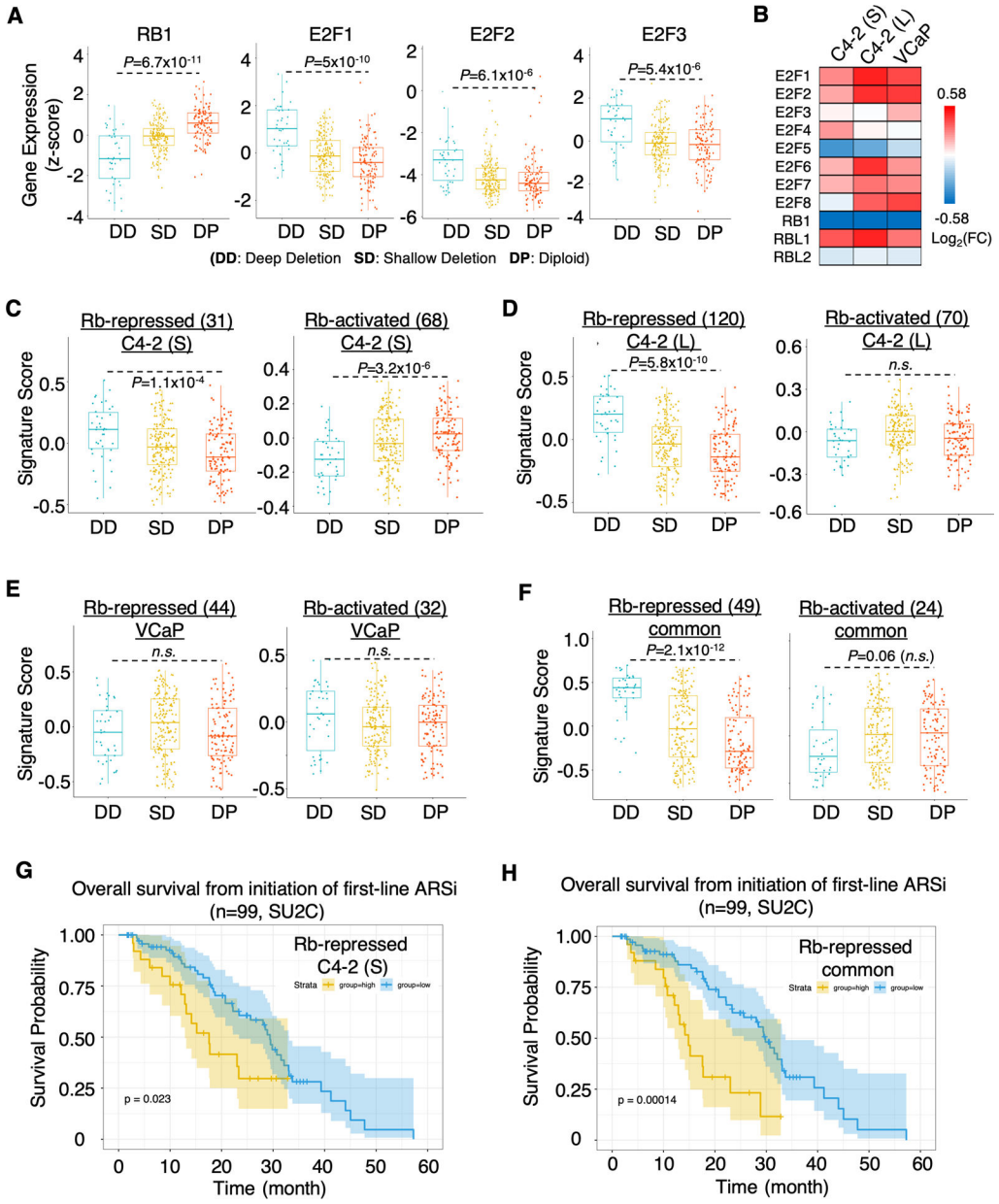

Figure 3. Increased expression of Rb directly repressed genes is associated with the aggressiveness of CRPC

(**A**) Gene expression of *RB1*, *E2F1*, *E2F2*, and *E2F3* in human mCRPC samples (SU2C cohort, Abida 2019) (*RB1* status: DD-Deep Deletion; SD-Shallow Deletion; DP-Diploid). (**B**) Heatmap view for a panel of *E2F* and *RB* family genes in C4–2-tet-shRB and VCaP cells. (**C**, **D**) Box plots for signature scores of Rb direct targets developed from C4–2-tet-shRB cells with short-term (C) or long-term (D) depletion of Rb (short-term repressed: 31-gene; short-term activated: 68-gene; long-term repressed: 120-gene; long-term activated: 70-gene; fold-change>1.3) in SU2C mCRPC dataset (different *RB1* genotype). (**E**) Box plots for signature scores of Rb direct targets developed from VCaP cells (repressed: 44-gene; activated: 32-gene; fold-change>1.5) in SU2C mCRPC dataset grouped by different *RB1* deletion status. (**F**) Box plots for signature scores of the common Rb targets developed from

both C4–2-tet-shRB cells (short-term Rb depletion) and VCaP cells (repressed: 49-gene; activated: 24-gene) in SU2C mCRPC dataset (different *RB1* genotype). (**G**, **H**) Kaplan–Meier analyses for the overall survival from the initiation of the first-line ARSi in the tumors with higher scores (yellow, top 25%) of the C4–2 Rb-target signature (short-term repressed) (G) or the common Rb-target signature (repressed) (H) versus with lower scores (blue, bottom 75%).

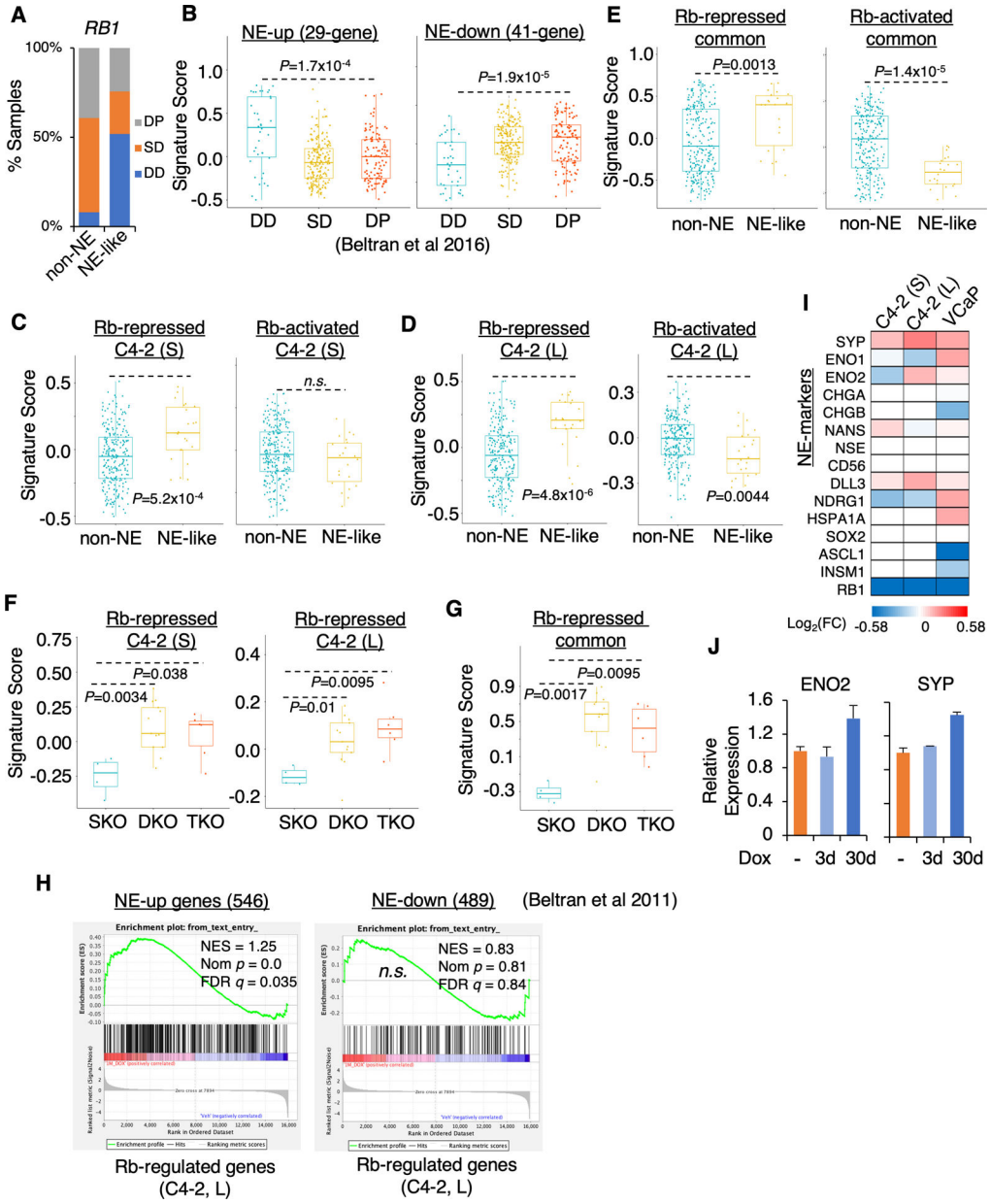

Figure 4. Rb directly repressed genes are upregulated in CRPC-NE

(**A**) Percentage of *RB1* genotype in SU2C mCRPC samples grouped by different neuroendocrine (NE) features (non-NE vs NE-like). (**B**) Box plots for signature scores of NE up/downregulated genes (Beltran 2016) in SU2C mCRPC dataset (different *RB1* genotype). (**C**, **D**, **E**) Box plots for signature scores of Rb directly repressed targets identified from C4–2-tet-shRB cells with short-term (C) or long-term (D) depletion of Rb or the common Rb-target genes (E) in SU2C mCRPC dataset (non-NE vs NE-like). (**F**, **G**) Box plots for signature scores of Rb direct targets identified from C4–2-tet-shRB cells (F) or the common Rb-target genes (G) in the RNA-seq dataset of murine PCa cell lines (SKO: $Pten^{-/-}$, DKO: $Pten^{-/-}/Rb1^{-/-}$, TKO: $Pten^{-/-}/Rb1^{-/-}/Trp53^{-/-}$). (**H**) GSEA showing enrichment of NE-regulated gene set (Beltran 2011) in Rb regulated genes (C4–2-tet-shRB, long-term Rb

depletion). (**I**) Heatmap view for a panel of NE markers in C4–2-tet-shRB and VCaP cells. (**J**) qRT-PCR for *ENO2* and *SYP* in C4–2-tet-shRB cells treated with doxycycline (3d or 30d, 0.05μg/ml).

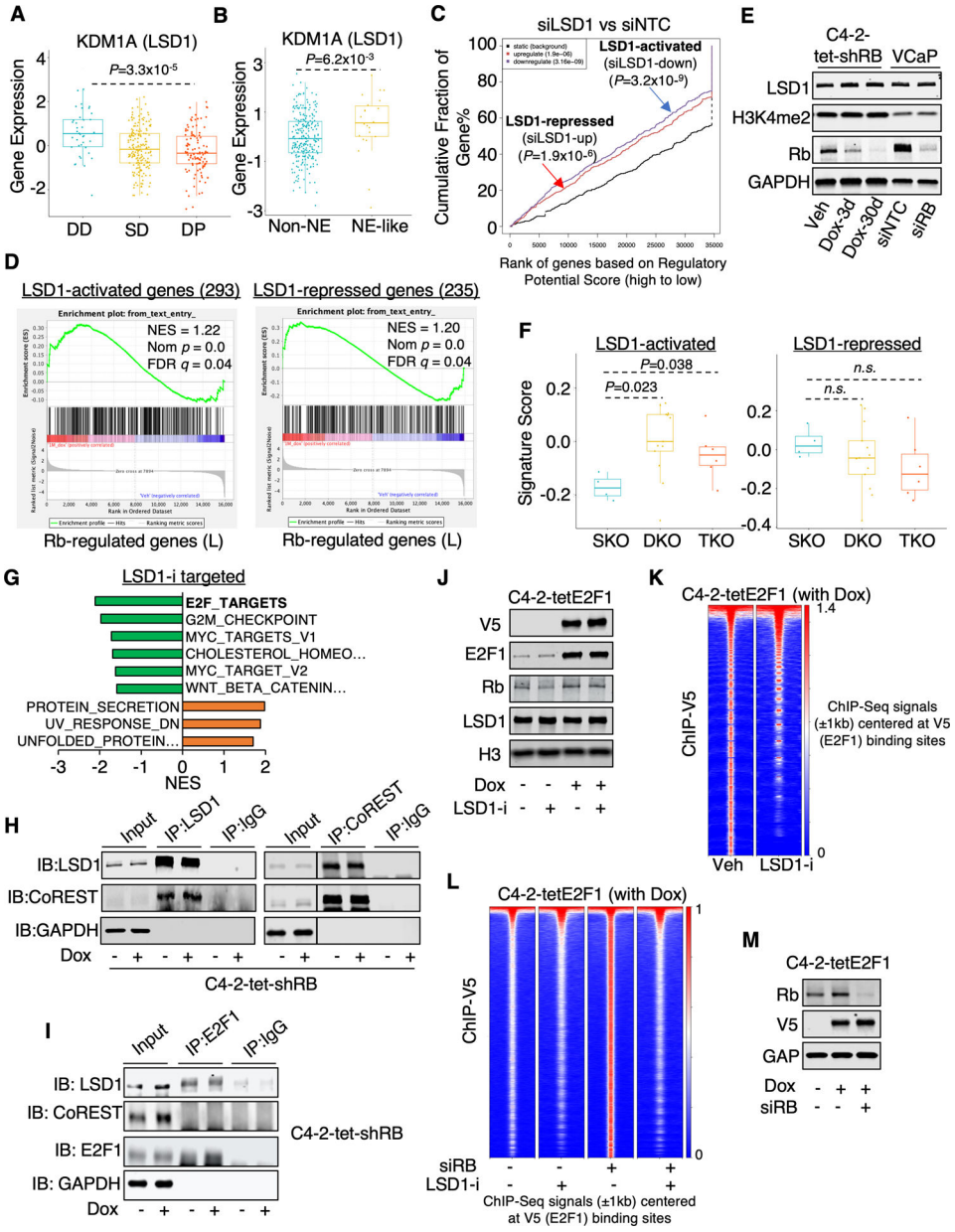

Figure 5. *RB1* loss increases the expression of LSD1-activated genes

(**A**, **B**) *KDM1A* (*LSD1*) expression in SU2C mCRPC samples grouped by different *RB1* genotype (A) or by NE features (B). (**C**) BETA for the association of LSD1 binding sites with the expression of LSD1-regulated genes (LNCaP cells). (**D**) GSEA revealed the enrichment of previously identified LSD1 directly activated and repressed gene sets (Cai 2014) in Rb-regulated genes (C4–2-tet-shRB cells, long-term). (**E**) Immunoblotting for LSD1, H3K4me2, and Rb in C4–2-tet-shRB cells and VCaP cells with or without *RB1* silencing. (**F**) Signature scores of LSD1 directly activated or repressed gene targets in SKO, DKO, and TKO cells. (**G**) GSEA revealed the significantly enriched hallmark gene sets (P<0.05) in LSD1 inhibitor (GSK2879552, 1μM for 2d) regulated genes (LNCaP cells). (**H**) Immunoblotting for CoREST and LSD1 proteins that were co-immunoprecipitated with

LSD1 and CoREST in C4–2-tet-shRB cells. (**I**) Immunoblotting for LSD1 and CoREST that were co-immunoprecipitated with E2F1. (**J**) Immunoblotting for indicated proteins in C4–2-tetE2F1 cells (expressing doxycycline-regulated V5-E2F1) treated with or without 50μM GSK2879552 and with/without doxycycline. (**K**) Heatmap view for ChIP-seq signal intensity of V5 (E2F1) centered at total V5 peaks in C4–2-tetE2F1 cells (pretreated with doxycycline for 2d) treated with/without GSK2879552 (50μM) for 24h. (**L**) Heatmap view for ChIP-seq signal intensity of V5 (E2F1) centered at total V5 peaks in C4–2-tetE2F1 cells (pretreated with doxycycline for 2d) transfected with siNTC versus siRB and then treated with or without GSK2879552 for 24h. **(M**) Immunoblotting for indicated proteins in C4–2-tetE2F1 cells treated with or without doxycycline and transfected with siNTC versus siRB.

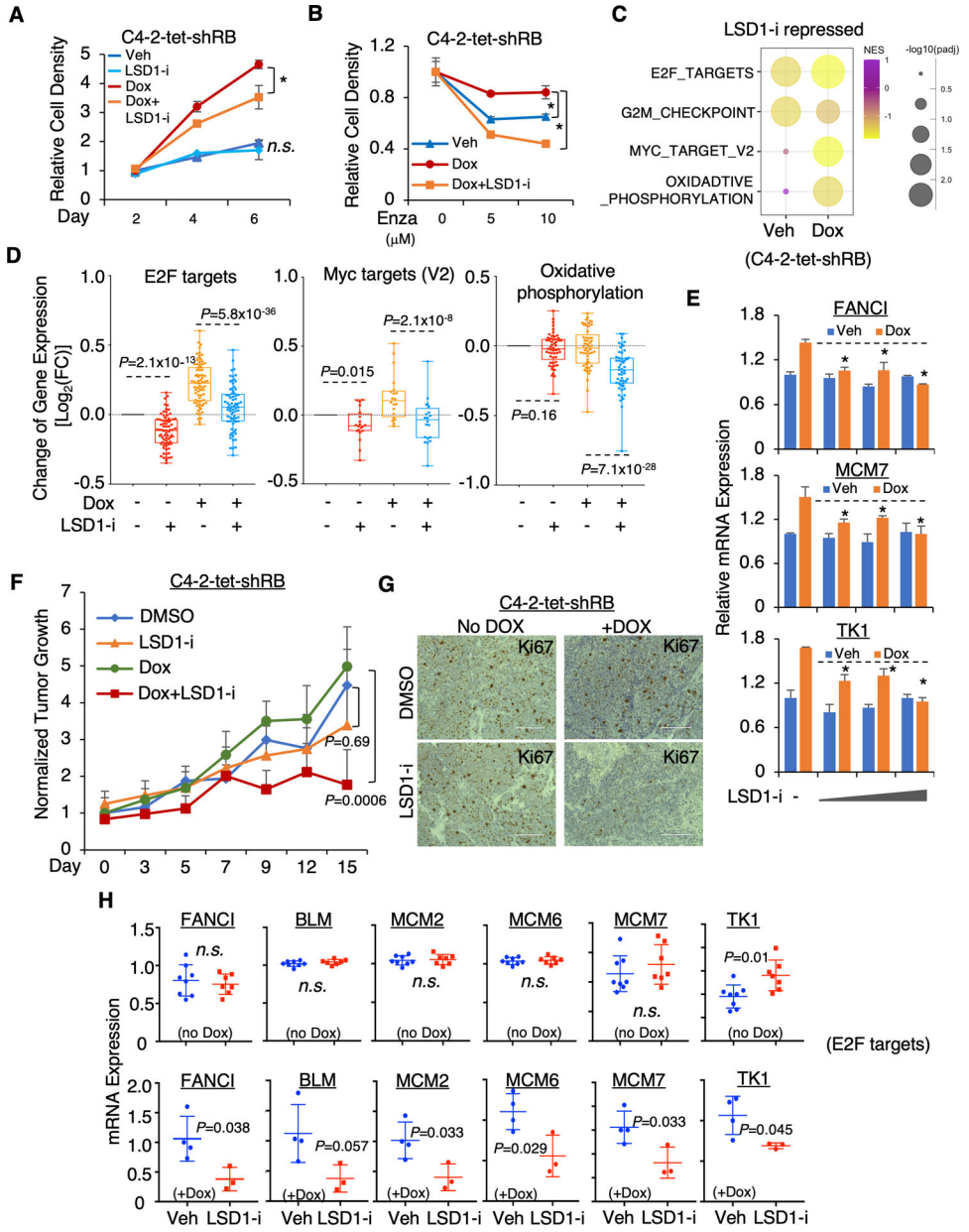

Figure 6. *RB1* loss sensitizes CRPC to LSD1 inhibition

(**A**) Cell proliferation assay for C4–2-tet-shRB treated with or without GSK2879552 (5μM) or doxycycline (0.05μg/ml). (**B**) Cell proliferation assay for C4–2-tet-shRB cells pretreated with doxycycline or GSK2879552 (5μM) and then treated with 0–10μM of enzalutamide (6d). (**C**) GSEA showing the significantly enriched hallmark gene sets (cutoff: $P<0.05$) in LSD1-i down-regulated genes in C4–2-tet-shRB cells (data obtained from RNA-seq; GSK2879552: 10μM, 24h; doxycycline: 3d). (**D**) Box plots for the change of expression levels of E2F targets, Myc targets (V2), or oxidative phosphorylation genes that were repressed by LSD1-i (with dox) in these samples were shown. (**E**) qRT-PCR for the mRNA expression of indicated E2F targets in C4–2-tet-shRB cells treated with 0–50μM GSK2879552 (24h) and with/out doxycycline (3d). (**F, G**) Tumor growth of C4–2-tet-shRB

xenografts (in castrated male SCID mice) treated with DMSO or GSK2879552 (33 mg/kg/day, intraperitoneal injection) in the absence of doxycycline or fed with doxycycline supplemented diet. Tumor growth was measured by caliper (F) and further examined by immunohistochemistry staining of Ki67 (G). (**H**) qRT-PCR for the mRNA expression of indicated E2F targets in tissue samples from xenograft tumors.